Optimal Thickness for Charge Transfer in Multilayer Graphene Electrodes

Marcelo A. Kuroda,* J. Tersoff, Razvan A. Nistor, and Glenn J. Martyna

IBM T. J. Watson Research Center, 1101 Kitchawan Road, Yorktown Heights, New York 10598, USA

(Received 3 January 2014; published 27 February 2014)

We study the charge transfer in multilayer graphene from first principles. We find that highly oriented (Bernal) and misoriented (turbostratic) multilayers show similar charge distributions despite their different electronic structure. We quantify the charge transfer and doping distribution in turbostratic graphene layers, where the screening is affected by vanishing density of states near the Fermi level. The results are in good agreement with an analytic model accounting for the electrostatic interaction and the band filling and point out the importance of system-specific interactions between the surface and the first layer. We find that graphene is an outstanding material for ultrathin electrodes, as most of the benefits of multilayer graphene can be captured with bilayers.

DOI: 10.1103/PhysRevApplied.1.014005

Since the isolation of individual graphene layers [1], a vast amount of research has explored new physics in these two-dimensional structures. The fabrication of large-scale sheets [2,3] has highlighted the potential of graphene for novel uses in photovoltaic applications [4], logic devices [5,6], flexible electrodes [7], molecule detection [8], and supercapacitors [9–12]. Understanding the charge transfer to multilayers graphene (MLG) is important for the realization of graphene-based devices, as it impacts the effective sheet conductance [1] in flexible electrodes and field-effect transistors or the storage in high-density supercapacitor applications.

Different fabrication methods lead to graphene multilayers with distinct stacking sequences. Mechanical exfoliation of highly oriented graphite [1] gives graphitic Bernal stacking. In contrast, growth from the C face of SiC [13,14] or assembly of CVD layers [15] gives a turbostratic (TS) structure with effective decoupling of the layers [16,17]. Despite the weak coupling, there is still significant interlayer conductance in TS graphene due to scattering processes [18]. Thus, the stacking order results in different electronic responses, such as those observed in Raman spectroscopy [19,20] and photocurrent microscopy [21] experiments. However, it is not clear how it affects the charge distribution across the layers.

Here we investigate the charge-transfer doping and interlayer screening in MLG systems using first-principles calculations. Surprisingly, we find that the total charge transfer to the graphene stack already reaches its maximum value after only two layers. This supports the potential of few-layer graphene as ultrathin electrodes. In addition, we observe that the induced charge distributions in highly oriented Bernal (AB) and TS MLG are similar despite their different dispersions near the Fermi level. For multilayers, the treatment of these issues has generally been limited to tight binding calculations for the AB stacking case [22] and simple analytical models for the TS stacking [23,24]. Our first-principles results provide a critical test of such models, identifying their strengths and limitations.

The charge-transfer doping in MLG can arise in response to a gate voltage or simply by charge transfer from an adjacent metal due to work function and chemical differences. In the present work, charge is induced by placing MLG in contact with a metal surface, as shown in Fig. 1(a). We choose magnesium (Mg) for the metal, as it has a large work function difference with graphene. Moreover, the metal in-plane lattice constant requires only a small artificial strain (∼1.4%) to be commensurate with the rotated $\sqrt{7} \times \sqrt{7}$ graphene cell. This supercell is sufficient to accommodate a simple model of TS graphene, with a 21.8° rotation between adjacent graphene layers. We fix in-plane and out-of-plane lattice constants of graphene to their experimental values ($a_0 \approx 2.46$ Å and $c_0 \approx 3.4$ Å, respectively), and in order to facilitate the comparison of the essential physics differentiating the AB and TS cases, the system is not relaxed. By rigidly varying the distance between the graphene and the metal (d_{mg}) we change the amount of charge transfer between the metal and graphene layers. The metal is represented by six Mg layers in the hcp crystal structure; a vacuum space of approximately 12 Å is left between the periodic repetitions of the supercell. This work is performed within the density functional theory using the local density approximation [25] as implemented in the Quantum ESPRESSO software package [26] and includes dipole correction for slab geometries [27]. In the calculations, cutoff energies of 75 and 300 Ry are employed for the wave function and density, respectively.

We first compare the charge distribution in the metal-graphene system for the AB and TS stacked multilayers. We define the plane-average charge density profile

*Present address: Department of Physics, Auburn University. Auburn, AL 36849, USA.
mkuroda@auburn.edu

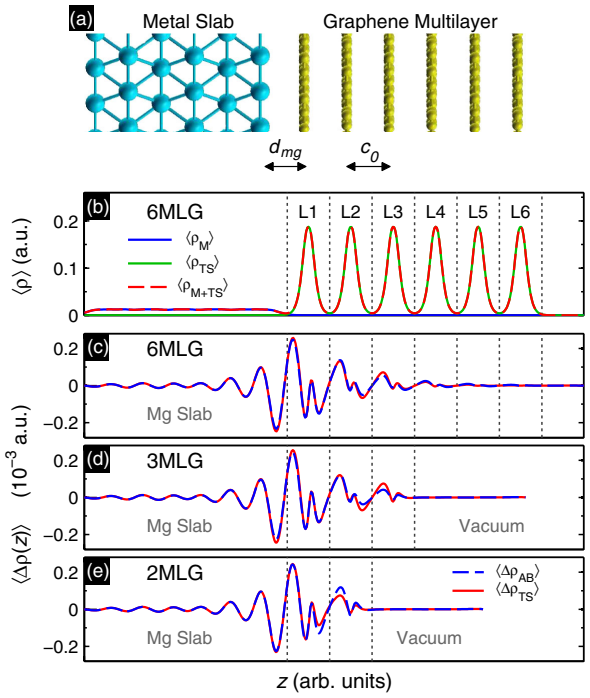

FIG. 1 (color online). (a) Schematic of a metal-MLG ($N = 6$) system. (b) Charge density profiles for the isolated metal $\langle\rho_M\rangle$ (blue), isolated ($N = 6$) TS MLG $\langle\rho_{\rm TS}\rangle$ (green), and metal-TS system $\langle\rho_{M+{\rm TS}}\rangle$ (red dashed line) for $d_{\rm mg} = 3.5$ Å. Vertical dotted lines indicate 3.4-Å-wide regions centered around each graphene layer. (c)–(e) Induced charge density $\langle\Delta\rho\rangle$ [Eq. (1)] for AB (blue dashed line) and TS (red line) MLG cases with $N = 6$, 3, and 2, respectively.

$$\langle\rho(z)\rangle = \frac{1}{A}\int_A \rho(\mathbf{r})dxdy, \tag{1}$$

where A is the area of the supercell parallel to the interface. For simplicity, we, henceforth, refer to this as $\langle\rho\rangle$, leaving the z dependence implicit. To make visible the charge rearrangements, which are very small compared to the total charge [Fig. 1(b)], we compute the total charge $\langle\rho_{M+G}\rangle$, but also the charge of the metal alone $\langle\rho_M\rangle$ and the graphene slab alone $\langle\rho_G\rangle$. We define the charge transfer $\langle\Delta\rho_G\rangle$ as

$$\langle\Delta\rho_G\rangle = \langle\rho_{M+G}\rangle - \langle\rho_M\rangle - \langle\rho_G\rangle. \tag{2}$$

We compare the results for $\langle\Delta\rho_{AB}\rangle$ and $\langle\Delta\rho_{\rm TS}\rangle$ with $N = 6$, 3, and 2 (Fig. 1). The charge transfer for $N = 6$ is nearly identical in the two cases, despite their different band structures [17]. The differences become more visible (though still small) for thinner films.

Figure 2 shows the band structure along the $\Gamma \to {\rm M} \to {\rm K} \to \Gamma$ symmetry lines of a bilayer graphene on metal with $d_{\rm mg} = 3.5$ Å, in the two different stacking orders. Because of the large size of the unit cell, multiple bands reside near the Fermi level ($E = 0$). We isolate the contribution of the graphene layers by computing the projections of the

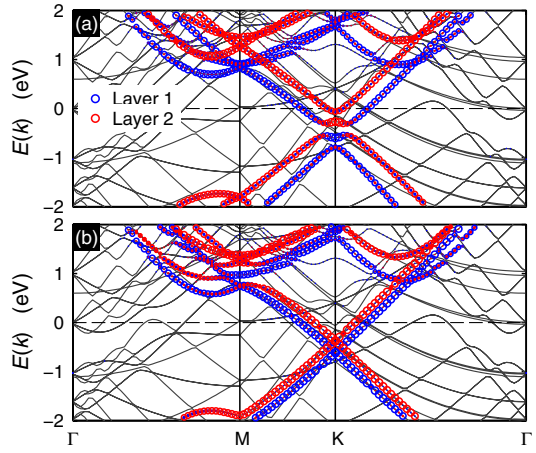

FIG. 2 (color online). Band structure (thin black lines) of bilayer graphene separated by 3.5 Å from a Mg surface: (a) AB and (b) TS stacking order, respectively. Circles superposed on bands show the projected weight of these bands onto carbon atomic orbitals of the first (blue) and second (red) graphene layers.

different Bloch states onto the carbon atomic orbitals. The area of the circles in Fig. 2 denotes the magnitude of the total projection onto a given graphene layer, and the color indicates whether the projection is onto atoms in the first or the second layer. Consistent with the work function difference ($\phi_G > \phi_{\rm Mg}$) all the cases show n doping of the graphene layers with most of the charge transferred to the adjacent layer.

The dispersion near the Fermi level for bilayer graphene is considerably different depending on the stacking order. The AB-stacked case [Fig. 2(a)] shows the opening of a band gap $\Delta \sim 0.2$ eV at the Dirac point (DP) as the presence of the metal induces a nonzero electric field between the layers [28–30]. In contrast, no significant gap appears for the TS stacking [Fig. 2(b)] where the band structure of the bilayer resembles that of individual graphene layers [17,31] (i.e., preserving the linear dispersion near the DP) shifted in energy due to the unequal doping on each of the layers.

As the number of layers increases, the band structure of MLGs [16,22,32] becomes more complex. As an example, Fig. 3 shows the case for six-layer MLG in the AB and TS stackings with $d_{\rm mg} = 3.5$ Å. From the projection onto the carbon atomic orbitals, in the AB stacking we observe two effects of the interaction between layers: it disrupts the linear dispersion near the DP, and it causes individual layers to have significant weight in more than one of the bands. This feature is more evident in the layers located far from the metal where the weak (screened) electrostatic potential leaves layers nearly degenerate in energy. In contrast, each layer in the TS case still exhibits the linear band structure of monolayer graphene due to the weak coupling between them [17].

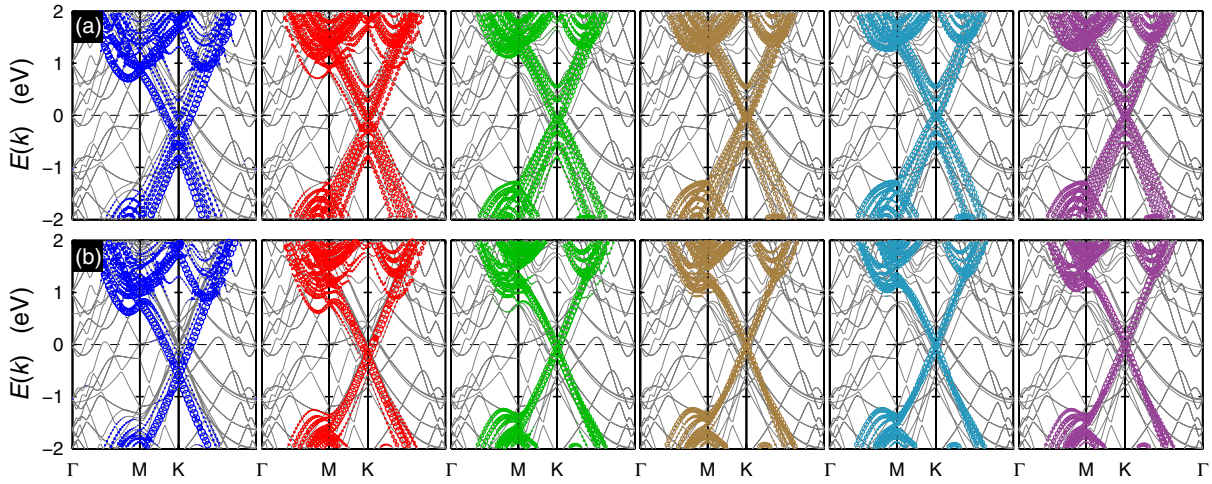

FIG. 3 (color online). Band structure (thin grey lines) of $N = 6$ MLG located at 3.5 Å from the metal surface for different stacking orders: (a) AB and (b) TS. Superposed symbols in the subplots denote the weight of the projections of bands onto carbon orbitals of each individual graphene layer (left, layer nearest to the metal; right, farthest layer).

To quantitatively analyze the doping in different layers, we wish to determine the net charge on each layer with some precision. For TS graphene, the net charge (doping) on the layer can be estimated from the energy position of the DP (E_{DP}) for that layer relative to the Fermi level (E_F) as

$$q = \pm \frac{1}{\pi} \left(\frac{E_{\mathrm{DP}} - E_F}{\hbar v_F} \right)^2, \tag{3}$$

where $\hbar$ is Plank's constant, v_F is the graphene Fermi velocity ($v_F \sim 1.1 \times 10^8$ cm/ sec), and the sign corresponds to the sign of $E_{\mathrm{DP}} - E_F$. As an example, the inset of Fig. 4 shows those projections in the vicinity of the Fermi level for the case previously depicted in Fig. 3(b). Each layer has a prominent projection where the DP is located, as well as a few less significant ones (denoted by smaller dots). This small degree of mixing is somewhat exaggerated by our model system, because to have a reasonable cell size requires alternate layers to have the same orientation. In true TS graphene, the layers are fully decoupled from their neighbors.

Figure 4 shows the charge distribution on each of the six layers computed using Eq. (2). To vary the total charge, we consider distances d_{mg} from 3.0, 3.5, and 4.0 Å. For a given d_{mg}, the charge distribution q_i is concentrated near the metal. Beyond the second layer, the charge is very small and stems from a small region of the Brillouin zone around the K point, so convergence with increasingly fine k-point mesh is extremely slow. In addition, convergence occurs oscillating between a strong and weak screening depending on whether the k-point grid contains or straddles the K point (12×12 or 16×16 grids in Fig. 4, respectively) due to the semimetal property of graphene. A more detailed description on the k-point convergence [33,34] is provided in the Supplemental Material [35].

Figure 4 also compares our first-principles results (solid triangles) with those obtained using an analytical model [23,24] (open symbols) in which the charge distribution in the MLG is determined by minimizing the energy arising from the contributions of electrostatic interaction between

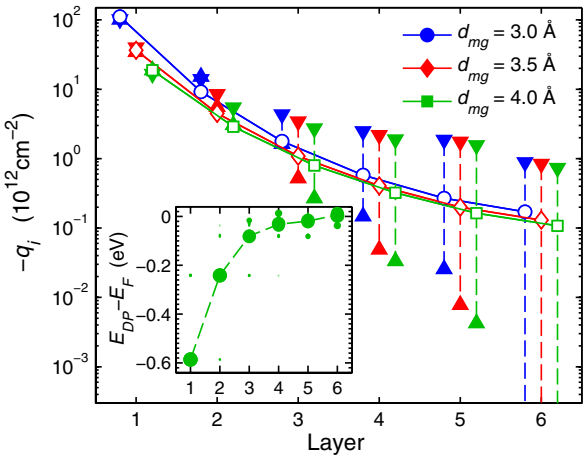

FIG. 4 (color online). Charge transfer to each of the six layers for different distances $d_{\mathrm{mg}} = 3.0$ (blue), 3.5 (red), and 4.0 Å (green). Triangles show the results from first-principles calculations, with two different types of k-point meshes: one that includes the K point (triangle up) and one that straddles it (triangle down). In the former case, the charge in the last layer actually reverses sign. For clarity, the different distances have been plotted with a small horizontal shift to avoid superposition of symbols, and a vertical dashed line is drawn between the first-principles results for different k samples. Open symbols show an analytical model [24]. Inset: Projection onto layer orbitals for states at the K point ($d_{\mathrm{mg}} = 3.5$ Å). Each dot denotes a state with energy indicated along the vertical scale with projection onto states in the ith layer (horizontal axis). The magnitude of the projection is represented by the area of the dot.

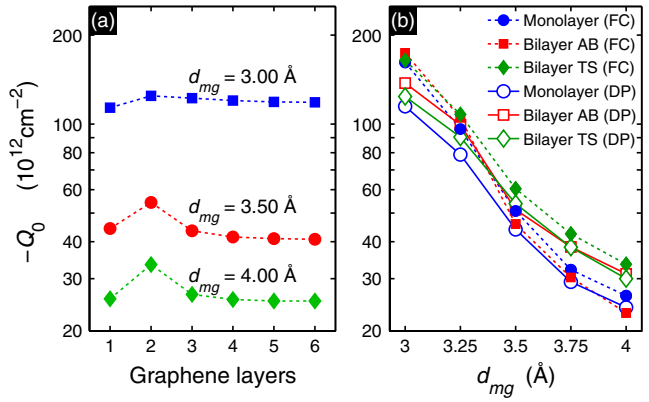

FIG. 5 (color online). (a) Total charge transfer (on logarithmic scale) to MLG as a function of the number of graphene layers, for values of $d_{\mathrm{mg}} = 3.0$, 3.5, and 4.0 Å. In each case, the maximum charge transfer to the graphene slab occurs for two layers. (b) Estimate of the charge transfer to monolayer (∘), AB bilayer (□), and TS bilayer (◇) as computed from the FC (open symbols) and the DP position (solid symbols).

layers and the band filling of each of the layers. The model has one parameter, the total charge ($Q_0 = \sum_{i=1}^{N} q_i$), which we take from the first-principles results. In the model, we use the same broadening [36] of 0.01 Ry used in the first-principles calculations.

The resulting charge distribution using the analytical model is in excellent agreement with the calculations. Far from the metal, where the first-principles results depend on the wave vector mesh, the model results are intermediate between the two types of meshes, as expected.

The total charge and its dependence on the layer thickness are important for graphene applications as ultrathin electrodes. In Fig. 5(a), we show the total charge Q_0 induced in the TS-stacked MLG systems as a function of the number of layers for three different distances d_{mg} (3.0, 3.5, and 4.0 Å). A peculiar feature is observed for a fixed distance d_{mg}: excluding the special case of a monolayer, the total charge decreases as the number of layers is increased. This unusual and counterintuitive behavior stems from the small induced charge in each additional graphene layer that reduces the quantum capacitance of the layer [37,38], thereby diminishing the overall quantum capacitance. The results suggest that two graphene layers are optimal for ultrathin electrodes.

Applying the analytical model to the present problem, we find that the maximum charge transfer actually occurs for a single layer, with the net charge decreasing monotonically with the number of layers. This surprising result reflects the dominant role of quantum capacitance. The reduced charge for a monolayer in our first-principles calculations stems from interactions between the metal surface and the first graphene layer [39] which have been omitted in analytical models.

These interactions are system specific, so the maximum charge may occur for a monolayer in some cases. Previous first-principles calculations for single-layer graphene physisorbed on different metals [39] show that even the type of doping (p or n) depends not only on the work function difference between the metal and the graphene but also on the distance between the graphene and the metal surface. Only for sufficiently large distances does the doping consistently correspond to that of the sign of work function difference. Furthermore, even in cases where the first layer is chemisorbed by the metal surface, subsequent layers preserve the graphenelike dispersion [40] and, thus, are expected to follow the same behavior.

Projections of Bloch states near the K point onto localized orbitals in different layers can form well-defined Fermi contours (FC) in systems where interlayer mixing is weak (TS stacking), or simple systems like bilayer AB [Fig. 2(a)]. In such cases, the surface area determined by the FC offers an alternative to compute the charge transfer to each layer. In Fig. 5(b), the charge transfer to monolayer and bilayer graphene where stacking order results in more prominent differences in the induced charges [Fig. 1(e)] is estimated both from the surface area of the FC (solid symbols) and the shift of the DP [41] (open symbols). The results show similar trends for the total change transferred as a function of the distance d_{mg}. The former approach yields somewhat larger results than the latter one (except for the AB bilayer at $d_{\mathrm{mg}} > 3.25$ Å). Such differences are expected, as deviations from the conical dispersion emerge when a large amount of charge is transferred. For a fixed distance, TS bilayers show a larger transfer than monolayers. AB bilayers show similar values to monolayers when using the FC method and similar to TS bilayers when employing the DP shift.

In summary, we study the electrostatic doping of MLG in contact with a metal surface using first-principles calculations. Our work shows that charge transfer is maximized with only one or two graphene layers, highlighting the potential of graphene as ultrathin electrodes. We find that for many-layer graphene, the induced charge distributions are nearly identical in Bernal and TS stacking, despite their different dispersion near the Fermi level. Charge distributions observed for TS MLG capture the features of nonlinear screening and stress the importance of the interactions with the surface missing in analytical models.

[1] K. S. Novoselov, A. K. Geim, S. V. Morozov, D. Jiang, Y. Zhang, S. V. Dubonos, I. V. Grigorieva, and A. A. Firsov, Electric field effect in atomically thin carbon films, Science **306**, 666 (2004).

[2] X. Li, W. Cai, J. An, S. Kim, J. Nah, D. Yang, R. Piner, A. Velamakanni, I. Jung, E. Tutuc, S. K. Banerjee, L. Colombo, and R. S. Ruoff, Large-area synthesis of high-quality and

uniform graphene films on copper foils, Science **324**, 1312 (2009).
[3] M. Segal, Selling graphene by the ton, Nat. Nanotechnol. **4**, 612 (2009).
[4] X. Wang, L. Zhi, and K. Mullen, Transparent conductive graphene electrodes for dye-sensitized solar cells, Nano Lett. **8**, 323 (2008).
[5] F. Xia, T. Mueller, Y. -M. Lin, A. Valdes-Garcia, and P. Avouris, Ultrafast graphene photodetector, Nat. Nanotechnol. **4**, 839 (2009).
[6] B. J. Kim, H. Jang, S.-K. Lee, B. H. Hong, J.-H. Ahn, and J. H. Cho, High-performance flexible graphene field effect transistors with ion gel gate dielectrics, Nano Lett. **10**, 3464 (2010).
[7] K. S. Kim, Y. Zhao, H. Jang, S. Y. Lee, J. M. Kim, K. S. Kim, J.-H. Ahn, P. Kim, J. -Y. Choi, and B. H. Hong, Large-scale pattern growth of graphene films for stretchable transparent electrodes, Nature (London) **457**, 706 (2009).
[8] F. Schedin, A. K. Geim, S. V. Morozov, E. W. Hill, P. Blake, M. I. Katsnelson, and K. S. Novoselov, Detection of individual gas molecules adsorbed on graphene, Nat. Mater. **6**, 652 (2007).
[9] M. D. Stoller, S. Park, Y. Zhu, J. An, and R. S. Ruoff, Graphene-based ultracapacitors, Nano Lett. **8**, 3498 (2008).
[10] J. J. Yoo, K. Balakrishnan, J. Huang, V. Meunier, B. G. Sumpter, A. Srivastava, M. Conway, A. L. M. Reddy, J. Yu, R. Vajtai, and P. M. Ajayan, Ultrathin planar graphene supercapacitors, Nano Lett. **11**, 1423 (2011).
[11] M. F. El-Kady, V. Strong, S. Dubin, and R. B. Kaner, Laser scribing of high-performance and flexible graphene-based electrochemical capacitors, Science **335**, 1326 (2012).
[12] E. Uesugi, H. Goto, R. Eguchi, A. Fujiwara, and Y. Kubozono, Electric double-layer capacitance between an ionic liquid and few-layer graphene, Sci. Rep. **3**, 1595 (2013).
[13] F. Varchon, R. Feng, J. Hass, X. Li, B. N. Nguyen, C. Naud, P. Mallet, J.-Y. Veuillen, C. Berger, E. H. Conrad, and L. Magaud, Electronic structure of epitaxial graphene layers on sic: Effect of the substrate, Phys. Rev. Lett. **99**, 126805 (2007).
[14] C. Faugeras, A. Nerriere, M. Potemski, A. Mahmood, E. Dujardin, C. Berger, and W. A. de Heer, Few-layer graphene on sic pyrolitic graphite, and graphene: A raman scattering study, Appl. Phys. Lett. **92**, 011914 (2008).
[15] A. Reina, X. Jia, J. Ho, D. Nezich, H. Son, V. Bulovic, M. S. Dresselhaus, and J. Kong, Large area, few-layer graphene films on arbitrary substrates by chemical vapor deposition, Nano Lett. **9**, 30 (2009).
[16] S. Latil and L. Henrard, Charge carriers in few-layer graphene films, Phys. Rev. Lett. **97**, 036803 (2006).
[17] S. Latil, V. Meunier, and L. Henrard, Massless fermions in multilayer graphitic systems with misoriented layers: Ab initio calculations and experimental fingerprints, Phys. Rev. B **76**, 201402 (2007).
[18] V. Perebeinos, J. Tersoff, and Ph. Avouris, Phonon-mediated interlayer conductance in twisted graphene bilayers, Phys. Rev. Lett. **109**, 236604 (2012).
[19] A. C. Ferrari, J. C. Meyer, V. Scardaci, C. Casiraghi, M. Lazzeri, F. Mauri, S. Piscanec, D. Jiang, K. S. Novoselov, S. Roth, and A. K. Geim, Raman spectrum of graphene and graphene layers, Phys. Rev. Lett. **97**, 187401 (2006).
[20] A. C. Ferrari, Raman spectroscopy of graphene and graphite: Disorder, electron-phonon coupling, doping and nonadiabatic effects, Solid State Commun. **143**, 47 (2007).
[21] A. Sagar, E. J. H. Lee, K. Balasubramanian, M. Burghard, and K. Kern, Effect of stacking order on the electric-field induced carrier modulation in graphene bilayers, Nano Lett. **9**, 3124 (2009).
[22] M. Koshino, Interlayer screening effect in graphene multilayers with *aba* and *abc* stacking, Phys. Rev. B **81**, 125304 (2010).
[23] S. S. Datta, D. R. Strachan, E. J. Mele, and A. T. C. Johnson, Surface potentials and layer charge distributions in few-layer graphene films, Nano Lett. **9**, 7 (2009).
[24] M. A. Kuroda, J. Tersoff, and G. J. Martyna, Nonlinear screening in multilayer graphene systems, Phys. Rev. Lett. **106**, 116804 (2011).
[25] J. P. Perdew and A. Zunger, Self-interaction correction to density-functional approximations for many-electron systems, Phys. Rev. B **23**, 5048 (1981).
[26] P. Giannozzi *et al.*, Quantum espresso: A modular and open-source software project for quantum simulations of materials, J. Phys. Condens. Matter **21**, 395502 (2009).
[27] L. Bengtsson, Dipole correction for surface supercell calculations, Phys. Rev. B **59**, 12301 (1999).
[28] E. McCann, Asymmetry gap in the electronic band structure of bilayer graphene, Phys. Rev. B **74**, 161403 (2006).
[29] H. Min, B. Sahu, S. K. Banerjee, and A. H. MacDonald, Ab initio theory of gate induced gaps in graphene bilayers, Phys. Rev. B **75**, 155115 (2007).
[30] E. V. Castro, K. S. Novoselov, S. V. Morozov, N. M. R. Peres, J. M. B. Lopes dos Santos, J. Nilsson, F. Guinea, A. K. Geim, and A. H. Castro Neto, Biased bilayer graphene: Semiconductor with a gap tunable by the electric field effect, Phys. Rev. Lett. **99**, 216802 (2007).
[31] S. Shallcross, S. Sharma, and O. A. Pankratov, Twist boundary in graphene: Energeticsand electric field effect, J. Phys. Condens. Matter **20**, 454224 (2008).
[32] H. Goto, E. Uesugi, R. Eguchi, and Y. Kubozono, Parity effects in few-layer graphene [Nano Lett. (to be published)], http://pubs.acs.org/doi/pdf/10.1021/nl402404z.
[33] O. Leenaerts, B. Partoens, and F. M. Peeters, Paramagnetic adsorbates on graphene: A charge transfer analysis, Appl. Phys. Lett. **92**, 243125 (2008).
[34] H. J. Monkhorst and J. D. Pack, Special points for Brillouin-zone integrations, Phys. Rev. B **13**, 5188 (1976).
[35] See Supplemental Material at http://link.aps.org/supplemental/10.1103/PhysRevApplied.1.014005 for a discussion on *k*-point convergence.
[36] M. Methfessel and A. T. Paxton, High-precision sampling for Brillouin-zone integration in metals, Phys. Rev. B **40**, 3616 (1989).
[37] T. Fang, A. Konar, H. Xing, and D. Jena, Carrier statistics and quantum capacitance of graphene sheets and ribbons, Appl. Phys. Lett. **91**, 092109 (2007).
[38] J. Xia, F. Chen, J. Li, and N. Tao, Measurement of the quantum capacitance of graphene, Nat. Nanotechnol. **4**, 505 (2009).

[39] P. A. Khomyakov, G. Giovannetti, P. C. Rusu, G. Brocks, J. van den Brink, and P. J. Kelly, First-principles study of the interaction and charge transfer between graphene and metals, Phys. Rev. B **79**, 195425 (2009).

[40] M. A. Kuroda, J. Tersoff, D. M. Newns, and G. J. Martyna, Conductance through multilayer graphene films, Nano Lett. **11**, 3629 (2011).

[41] The DP position in AB bilayers is extrapolated from the cone.